Available online at www.sciencedirect.com
ScienceDirect
Journal of Power Sources 175 (2008) 372–382
JOURNAL OF POWER SOURCES
www.elsevier.com/locate/jpowsour

DMFC anode polarization: Experimental analysis and model validation

A. Casalegno *, R. Marchesi

Dipartimento di Energetica, Politecnico di Milano, Piazza Leonardo da Vinci 32, 20133 Milano, Italy

Received 5 July 2007; received in revised form 3 September 2007; accepted 5 September 2007
Available online 11 September 2007

Abstract

Anode two-phase flow has an important influence on DMFC performance and methanol crossover. In order to elucidate two-phase flow influence on anode performance, in this work, anode polarization is investigated combining experimental and modelling approach. A systematic experimental analysis of operating conditions influence on anode polarization is presented. Hysteresis due to operating condition is observed; experimental results suggest that it arises from methanol accumulation and has to be considered in evaluating DMFC performances and measurements reproducibility. A model of DMFC anode polarization is presented and utilised as tool to investigate anode two-phase flow. The proposed analysis permits one to produce a confident interpretation of the main involved phenomena. In particular, it confirms that methanol electro-oxidation kinetics is weakly dependent on methanol concentration and that methanol transport in gas phase produces an important contribution in anode feeding. Moreover, it emphasises the possibility to optimise anode flow rate in order to improve DMFC performance and reduce methanol crossover.

Keywords: Fuel cell; DMFC; Model; Biphase; Validation

1. Introduction

Hydrogen polymer electrolyte membrane fuel cell (PEMFC) is considered a highly promising technology, especially for micro power generation and vehicular applications, due to its important attributes: low temperature and low pressure operation, no liquid electrolyte, high power density. The direct methanol fuel cell (DMFC) technology is a further development of PEMFC, particularly promising for portable electronics and vehicular applications, due to the advantage of a liquid fuel. Its main drawbacks are efficiency and power density lower than PEMFC. These topics are intensively studied [1,2] and are mainly attributed to methanol permeation through the polymer membrane and slow electrochemical methanol oxidation. The influence of anode two-phase flow is generally less investigated, despite its effect on DMFC performance and methanol crossover flux is very important. Experimental studies indicate degradation of cell performance under intensive generation of bubbles in the flow field [3–5]. Different works investigated operating conditions influence on anode polarization [7–9], but generally measurement uncertainty and reproducibility are not evaluated. Due to the complexity and the time needed for a whole experimental investigation numerical models have been adopted by some authors to investigate DMFC behaviour. But also recent state-of-the-art numerical models of DMFC present difficulties in rigorous description of the two-phase flow [10,11]. Kulikovsky developed a DMFC model [12], describing the two-phase flow in the anode channel, with an adaptive parameter, showing that under moderate methanol and oxygen stoichiometry the bubbles reduce limiting current density of the cell considerably. Ge presented a three-dimensional two-phase flow model [13], assuming only carbon dioxide presence in anode gas phase, and showed the influence of anode two-phase regime on methanol crossover. Wang presented a complete two-dimensional two-phase model, solved with a CFD technique, validated on a limited set of experimental measures [14].

This work aims to investigated anode polarization, in particular to produce a better understanding of two-phase flow influence on anode performance. A combined experimental and modelling approach is proposed. A systematic experimental analysis is reported, measurements are traceable to the international ref-

* Corresponding author.
E-mail addresses: andrea.casalegno@polimi.it (A. Casalegno), renzo.marchesi@polimi.it (R. Marchesi).

0378-7753/$ – see front matter © 2007 Elsevier B.V. All rights reserved.
doi:10.1016/j.jpowsour.2007.09.003

Nomenclature

c_{ref}	reference concentration (mol cm^{-3})
C	species concentration in channel (mol cm^{-3})
$\bar{C}$	time-averaged concentration in channel (mol cm^{-3})
C_t	species concentration in catalyst layer (mol cm^{-3})
D_b	effective diffusivity in diffusion layer (cm^2 s^{-1})
D_m	effective diffusivity in membrane (cm^2 s^{-1})
E_0	ideal potential difference (V)
F	Faraday constant (C mol^{-1})
h	channel height and width (cm)
i	local current density (A cm^{-2})
i_*	exchange current density (A cm^{-3})
k	Tafel constant (A cm^{-2})
K_H	Henry constant (mol J^{-1})
l_b	diffusion layer thickness (cm)
l_t	catalyst layer thickness (cm)
l_m	membrane thickness (cm)
L	channel length (cm)
M	molecular weight (g mol^{-1})
$\dot{m}$	inlet mass flow rate (g min^{-1})
N_{cross}	crossover flux (mol cm^{-2} s^{-1})
n_d	drag coefficient
p_{sat}	saturation pressure (MPa)
P	channel pressure (Pa)
R	universal gas constant (J mol^{-1} K^{-1})
R_c	contact resistance (Ω cm^2)
T	fuel cell temperature (K)
v	local velocity in channel (cm s^{-1})
V_{cell}	cell potential difference (V)
x	x coordinate (cm)
y	y coordinate (cm)
z	z coordinate (cm)

Greek symbol

α	Tafel transport coefficient
ϵ	volumetric void fraction
η	polarization (V)
γ	reaction order
ρ	compound density (g cm^{-3})
σ_m	membrane conductibility (Ω^{-1} cm^{-1})

Superscript

a	relative to anode
G	relative to gas phase
L	relative to liquid phase

Subscript

CO_2	relative to carbon dioxide
H_2O	relative to water
in	relative to channel inlet
Met	relative to methanol
out	relative to channel outlet

erence standard and are characterised in terms of uncertainty. This complete experimental characterisation permits to validate part of the model published in [15], analysing accurately model residuals and comparing them with experimental uncertainty.

Both the experimental analysis and the accurate model validation permit to produce a solid interpretation of the main phenomena involved in DMFC operation, contributing to optimise operating conditions and components.

2. Experimental equipment

The experimental setup is composed of a DMFC hardware, having a maximum cross-sectional area of 25 cm^{2}and a unique membrane electrode assembly (MEA) with an effective area of 12.25 ± 0.5 cm^2. The MEA is contained between two graphite blocks in which flow distributors are cut out (single serpentine channel, square section: depth 0.8 mm, width 0.8 mm, length 1500 mm). The cell is held together with two stainless steel plates using eight retaining bolts, which were closed applying a torque of 12 ± 0.5 N m.

To accommodate a calibrated thermocouple (uncertainty 0.05 K), connected both with a temperature controller and an acquisition system, a slot is present in the cathode steel plate. Two electrical heaters are placed within the steel plates, one for each electrode, to control the cell temperature. The graphite blocks present electrical contacts with gold plates, connected to a high accuracy power supply (current uncertainty 0.1% of the effective value + 0.012 A; voltage uncertainty 0.05% + 0.008 V). The anode solution is fed by a peristaltic pump with a resolution of 1 rpm and a speed uncertainty of 0.5%; anode mass flow rate is measured with an uncertainty of 1%. The methanol solutions were produced once, at the beginning of the experimentation, mixing bidistilled water and methanol (grade 99.5%$_{mass}$) and measuring the solution mass fractions (uncertainty 0.05%$_{mass}$) with a calibrated balance (uncertainty 0.1 g). Hydrogen, produced by a water electrolyzer (grade 99.999%$_{mole}$), is supplied to cathode side, as a reference electrode; its flow rate, constant at 0.2 N dm^3 min^{-1} is controlled and measured by a calibrated flowmeter (uncertainty 0.002 N dm^3 min^{-1}).

The MEA membrane is GEFC-117, anode catalyst layer (thickness 10 μm) presents a metal loading of 4 mg cm^2 (Pt:Ru = 2 on weight basis), cathode catalyst layer (thickness 10 μm) presents a metal loading of 4 mg cm^2 (Pt), anode and cathode diffusion layers are carbon paper (thickness 100 μm), cell gaskets consist of a Mylar layer (thickness 100 μm), in contact with the membrane, and a fibreglass layer (thickness 150 μm), covered by PTFE. The MEA was activated through a conditioning procedure, that consists of operating periods of 30 min at constant temperature (343 K) and load (0.6 V), with feeding of hydrogen (0.2 ± 0.002 N dm^3 min^{-1}) and air (2 ± 0.02 N dm^3 min^{-1}) saturated by water at 353 K and ambient pressure, for a total duration of 18 h subdivided equally in 3 days.

The described equipment permits thus to determine anode polarization, because cathode is considered a reference electrode, in particular a pseudo-DHE (dynamic hydrogen electrode) [6], whose potential is nearly constant and negligible in com-

parison to anode, when determining anode polarization curves. Therefore, measured voltage variations are mainly attributable to anode and membrane overpotentials, as described in [7], and the following polarization curves are reported versus reversible hydrogen electrode.

An acquisition procedure was developed to determine anode polarization characteristics for defined operating conditions and to permit measurement reproducibility evaluation. It includes two steps: initial transitory and characteristic acquisition. The initial transitory consists in an acquisition period, performed in the investigated operating conditions, fixing the voltage at 0.5 V, measuring voltage and current at 1 Hz frequency for 15 min; it is preceded by a preliminary not acquired transitory period of 15 min. The characteristic acquisition is composed of 22 single point measurements referred to different voltages (from 0.25 to 0.75 V, stepped by 0.05 V), collected following two one-way curves respectively increasing and decreasing voltage. Each single point acquisition is performed at constant voltage, measuring voltage and current at 1 Hz frequency for 400 s. Reproducibility procedure is composed of an initial transitory and two single point acquisitions, performed at 0.4 and 0.6 V.

Data obtained by a single point acquisition (two series of 400 values, voltage and current) are elaborated in two steps: transitory elimination and outliers elimination. The first 60 values are discarded, because resulting from the transitory caused by voltage variation. A robust method is used to individuate outliers. It eliminates values not included in the interval median $\pm$ 3 times standard deviation, estimated through median absolute deviation. Finally, the last 180 points are selected as significant, then mean values of voltage and current are calculated [16,17].

Measurement uncertainty of current is evaluated according to [16,17]. The contribution of each controlled parameter is evaluated considering the uncertainty of each measuring device and estimating experimentally its influence on current. The final current uncertainty results in the geometric sum of the uncertainties produced by the different controlled parameters. The single point uncertainty, u_i, (179 dof, 95% population) for current density i from 0 to 1.1 A cm^{-2}, is estimated equal to:

$$u_i = -5.8 \times 10^{-2} i^2 + 6.8 \times 10^{-2} i + 6 \times 10^{-3} \quad (1)$$

3. Analysis of experimental results

The following work refers to the experimental results of eight anode characteristic curves, whose operating conditions are reported in Table 1. The aim of the analysis is the investigation of operating conditions influence on anode polarization.

3.1. Hysteresis

Comparing two one-way characteristics, obtained increasing and decreasing voltage as previously described, a hysteresis phenomenon is observed; two examples are shown in Fig. 1. For high voltages the difference between the two average current densities has a magnitude order of 10^{-2}A cm^{-2}, similar to the typical uncertainty of single point current measurement. In some cases, the differences are statistically significant, as confirmed by the analysis of variance (ANOVA), and the two mean values have to be considered different. The differences are significant exclusively at high current density, in particular where fuel utilisation is above 80%. It is interesting to observe that during the backward curve, decreasing voltage, the current is lower than during the forward curve. The hysteresis may be caused by the following three factors: methanol, CO_2 or water accumulation. In the complete set of experimental data, the hysteresis results statistically significant exclusively when the fed solution has a concentration of 3.25 wt.%.

Table 1
Controlled parameters of experimental sessions

Session	Methanol concentration (wt.%) (uncertainty 0.07 wt.%)	Cell temperature (K) (uncertainty 0.05 K)	Anode flow rate (g/min) (uncertainty 1%)
1	3.25	332.9	0.47
2	3.25	333.1	1.08
3	3.25	353.6	0.47
4	3.25	353.3	1.08
5	6.5	332.7	0.47
6	6.5	332.8	1.08
7	6.5	352.7	0.47
8	6.5	352.7	1.08

With a solution concentration equal to 6.5 wt.% instead the hysteresis is not significant, as evident in Fig. 2. The curves at 6.5 wt.% reach higher current densities, thus a more intense CO_2 production and concentration, implying that hysteresis is not due to CO_2 accumulation, that in principle could reduced active fuel cell area. Moreover, at higher current density void fraction at anode increases, reducing water availability, allowing to exclude that hysteresis is caused by local membrane dehydration.

The previous considerations seem to individuate the cause of hysteresis in some sort of long-term methanol accumulation, coherently with [18]: during forward curve accumulated methanol is available to be consumed, on the contrary during backward curve there is methanol lack. This conclusion does not pretend to be exhaustive, further experimental analyses are needed to produce a more rigorous quantitative demonstration.

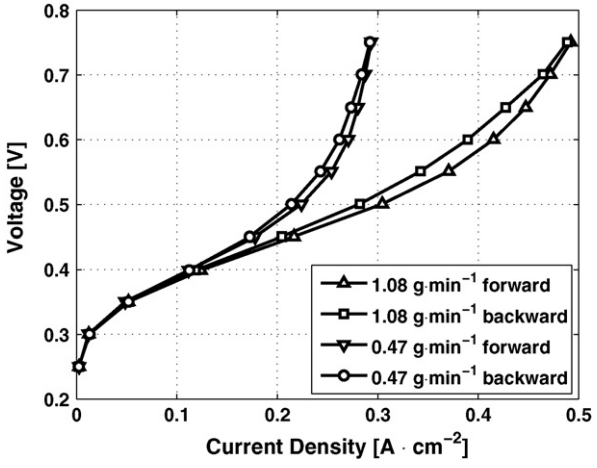

Fig. 1. Hysteresis in polarization curves. Fuel cell temperature: 333 K; methanol concentration: 3.25 wt.%.

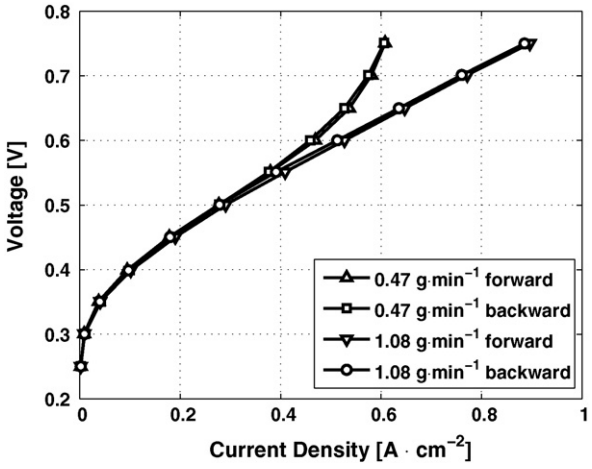

Fig. 2. Hysteresis in polarization curves. Fuel cell temperature: 333 K; methanol concentration: 6.5 wt.%.

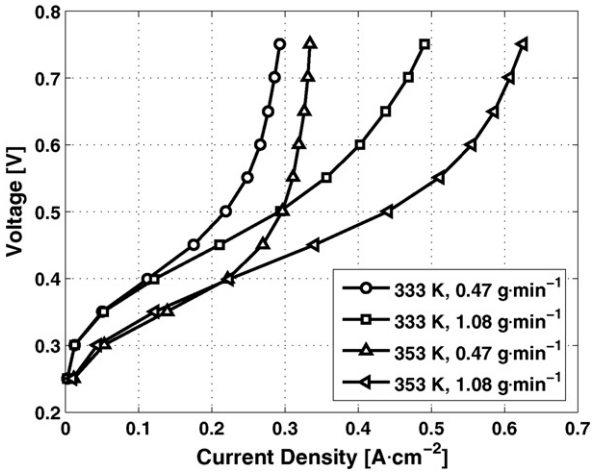

Fig. 4. Polarization curve. Methanol concentration: 3.25 wt.%; varying anode flow rate and fuel cell temperature.

Consequently hysteresis depends on operating condition history and have to be considered in evaluating the uncertainty of the mean values between forward and backward curves. Prudently final current density uncertainty, Eq. (1), is expanded by a factor equal to 1.7, compared to single point uncertainty; in this way ANOVA confirms that hysteresis effect is no more statistically significant.

3.2. Reproducibility

Reproducibility analysis is necessary to characterise properly the measures and to verify their reliability. Five reproducibility measures were carried out each in a different day for every polarization curve reported in this work; in Fig. 3 an example is reported, indicating current density measures in different days, their average value and uncertainty.

Current density variation between different days has generally a magnitude order of 10^{-3} A cm^{-2}, inferior than single point uncertainty. In few cases, around 10% of the analysed data, ANOVA reveals significant differences between days, considering single point uncertainty, not expanded by hysteresis factor. Taking into account the prudently adopted hysteresis factor, no differences between days are significant and reproducibility is demonstrated.

3.3. Operating conditions influence

In Figs. 4 and 5, four polarization curves at fixed methanol concentration are compared. The expected influence of temperature and anode flow rate is observed [7–9,19,20]: increasing temperature, methanol oxidation kinetics is enhanced, due to a reduction of activation losses; increasing anode flow rate, limiting current is higher and concentration losses reduce. Moreover, it is interesting to evidence that at 353 K the limiting currents result higher at the same anode flow rate and methanol concentration, thus fuel utilisation increases. This behaviour can be explained considering that at high temperature methanol evaporation and transport through gas phase is enhanced, increasing

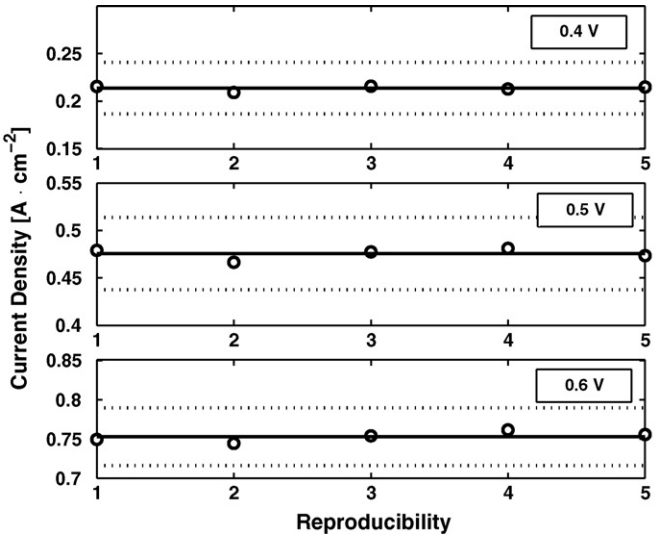

Fig. 3. Reproducibility measures in five different days. Fuel cell temperature: 353 K; methanol concentration: 6.5 wt.%; anode flow rate: 1.08 g min^{-1}.

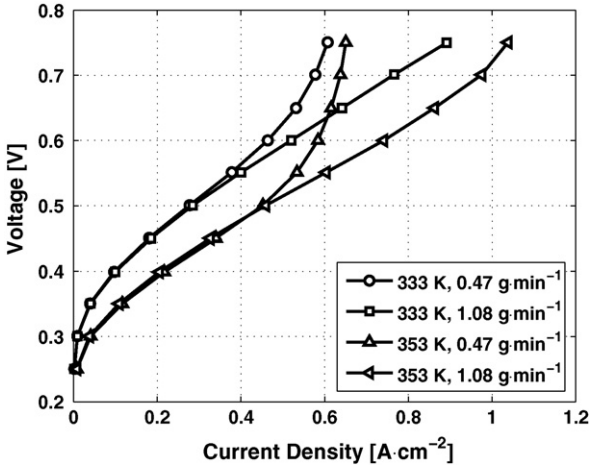

Fig. 5. Polarization curve. Methanol concentration: 6.5 wt.%; varying anode flow rate and fuel cell temperature.

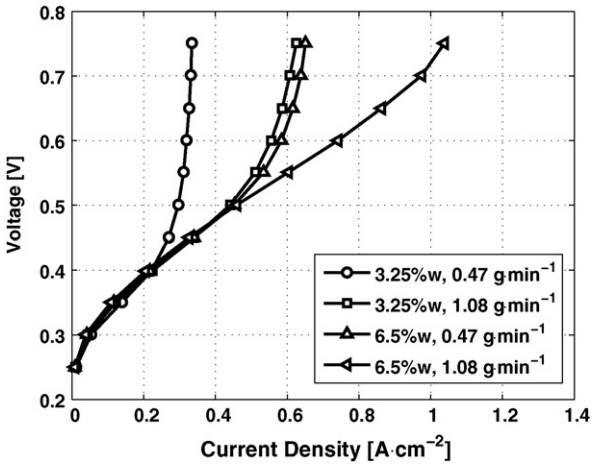

Fig. 6. Polarization curve. Fuel cell temperature: 353 K; varying methanol concentration and anode flow rate.

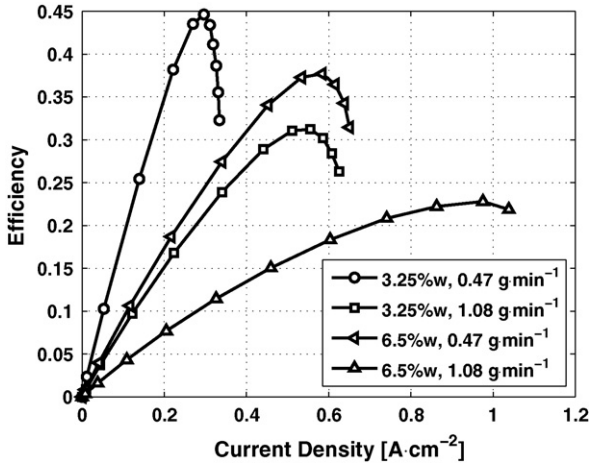

Fig. 8. Efficiency. Fuel cell temperature: 353 K; varying methanol concentration and anode flow rate.

methanol availability, despite its crossover increases due to an increase in membrane permeability.

Varying anode flow rate and methanol concentration at a fixed temperature, Fig. 6, it is evident that methanol electro-oxidation kinetics is weakly dependent on methanol concentration. Despite important variations in methanol concentration and anode flow rate, the polarization curves are very similar at low current, confirming that activation losses do not depend strongly on methanol concentration [8,9,19]; the main observed effects are due to concentration losses at high current density and methanol utilisation.

In Fig. 7, anode performances at constant effective methanol flow rate, defined as the product of anode flow rate times methanol concentration, are compared. At a constant temperature of 353 K the curves are very similar, implying that methanol availabilities in the two feeding configuration are comparable. At 333 K the behaviour is different: a higher methanol concentration permits to reach higher limiting current. This can be interpreted considering that at lower temperatures methanol availability in gas phase is reduced, confirming the important role of gas phase methanol transport in feeding the electrode.

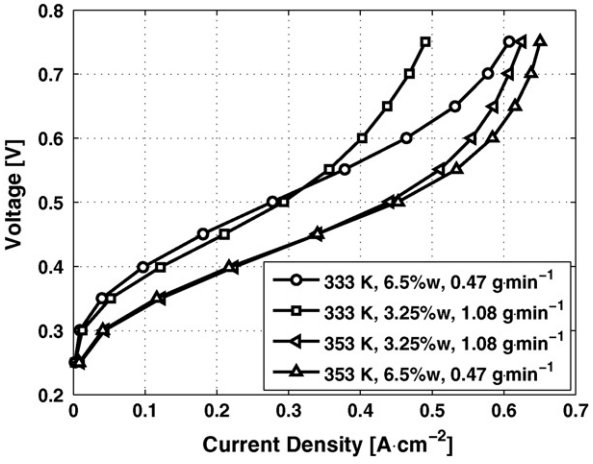

Fig. 7. Polarization curve. At similar effective methanol flow rate.

The fuel cell efficiency of methanol electrolysis can be defined, without considering eventual methanol recirculation, as the ratio between the effective produced power, equal to produced hydrogen power minus electrical power consumption, and the power related to inlet methanol flow rate:

$$\eta = \frac{(E_0 - V_{\text{cell}})I}{\dot{m}^{\text{a}} C^0_{\text{met}} LHV_{\text{met}}} \tag{2}$$

The maximum efficiency reached in the set of experimental data is around 45%, Fig. 8, without considering eventual fuel recirculation. Moreover, at similar methanol flow rate the efficiency results higher at a higher concentration and lower anode flow rate, confirming that the losses typically observed at high concentration in fuel cell operation are only due to cathode polarization, caused by methanol crossover.

4. Model validation

4.1. Model description

4.1.1. Assumptions

The model does not pretend to be a rigorous and exhaustive description of complex DMFC behaviour, but aims to reproduce the main involved phenomena and consequently to be a tool for DMFC understanding and optimization. The model is based on the following assumptions, already reported in [10–14,23–25]:

(1) The fuel cell hardware to be modelled has single serpentine square section distributors. The modelling domain is simplified as: a straight channel, anode distributor, and the MEA fed by it, Fig. 9. Coherently with the hardware anode gas channel height and width are equal, h^{a}, and MEA width is two times h^{a}. The MEA is composed by three sub domains: anode diffusion layers, catalyst layers and the membrane. The overall MEA area is assumed active. No reactions occur at cathode side.
(2) The modelling domain is assumed isothermal.
(3) The model neglects 2D and 3D effects; only convective transport is considered in the channel, along x direction;

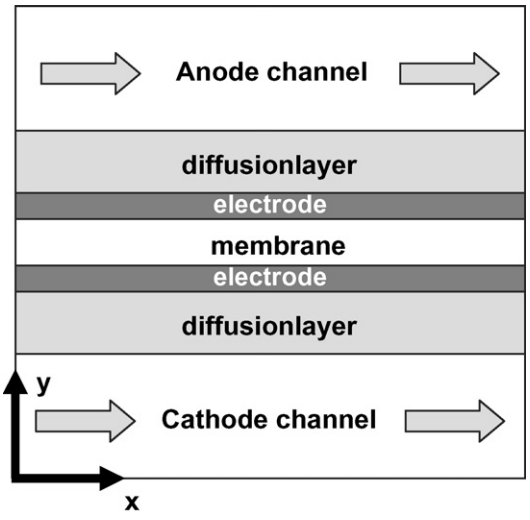

Fig. 9. Fuel cell scheme.

only diffusive transport takes place in y direction within diffusion layer and membrane; concentrations in catalyst layer are assumed constant.

(4) Three compounds, methanol, water and carbon dioxide, are considered in two phases at anode side.

(5) The anode two phase flow is simplified as a plug flow, where plugs and bubbles have the same velocity, constant within yz planes, as are species concentrations. Due to alternating plugs and bubbles single species concentrations in a certain volume are rapidly varying as time function, from the concentration in the liquid plug to the concentration in the bubble. Time-averaged local concentration of methanol, water and carbon dioxide, indicated as $\bar{C}$, are introduced to describe this behaviour at anode side.

(6) Gases, liquids and mixtures have an ideal behaviour. At anode side the concentration of the species, present in gas and liquid phases, are in equilibrium. Diffusion and catalyst layer porous structure do not influence single species gas-liquid equilibrium and void fraction.

(7) Anode pressure is assumed constant.

(8) The membrane is considered perfectly hydrated, due to high water stoichiometry at anode side.

(9) Methanol and water crossover are due to diffusion through the membrane and electro-osmosis. Methanol and water diffusion is promoted by their concentrations in liquid phase, as some experimental analysis suggest [7,21]. Membrane permeability to gaseous compounds is neglected, in particular carbon dioxide permeation through the membrane is negligible [22].

(10) Electrochemical reaction kinetics obey Tafel equation.

4.1.2. Anode channel

Taking into account the presented assumptions the species equations for methanol, carbon dioxide and water assume the following forms:

$$\frac{h^{\mathrm{a}}}{2}\frac{\partial(v^{\mathrm{a}}\bar{C}^{\mathrm{a}}_{\mathrm{Met}})}{\partial x} = -\frac{i}{6F} - N^{\mathrm{Met}}_{\mathrm{cross}} \tag{3}$$

$$\frac{h^{\mathrm{a}}}{2}\frac{\partial(v^{\mathrm{a}}\bar{C}^{\mathrm{a}}_{\mathrm{CO_2}})}{\partial x} = \frac{i}{6F} \tag{4}$$

$$\frac{h^{\mathrm{a}}}{2}\frac{\partial(v^{\mathrm{a}}\bar{C}^{\mathrm{a}}_{\mathrm{H_2O}})}{\partial x} = -\frac{i}{6F} - N^{\mathrm{H_2O}}_{\mathrm{cross}} \tag{5}$$

where v^{a} is the local velocity in x direction. Locally the convective flow of each species has a gradient equal to the sum of fluxes in y direction, caused by the anodic electrochemical reaction, in function of current density i, and by the crossover flux through the membrane. The factor $h^{\mathrm{a}}/2$ is due to assumption (1) and determines that MEA active area is equal to $2h^{\mathrm{a}}L$. Boundary conditions are related to species inlet flows, their values are reported in Table 3.

Time-averaged local concentration of methanol, water and carbon dioxide are defined as the sum of gas phase concentration, C^{G}, times volumetric gas fraction ϵ and liquid phase concentration, C^{L}, times volumetric liquid fraction $1-\epsilon$:

$$\bar{C}_{\mathrm{Met}} = \epsilon C^{\mathrm{G}}_{\mathrm{Met}} + (1-\epsilon)C^{\mathrm{L}}_{\mathrm{Met}} \tag{6}$$

$$\bar{C}^{\mathrm{a}}_{\mathrm{CO_2}} = \epsilon C^{\mathrm{a,G}}_{\mathrm{CO_2}} + (1-\epsilon)C^{\mathrm{a,L}}_{\mathrm{CO_2}} \tag{7}$$

$$\bar{C}^{\mathrm{a}}_{\mathrm{H_2O}} = \epsilon C^{\mathrm{a,G}}_{\mathrm{H_2O}} + (1-\epsilon)C^{\mathrm{a,L}}_{\mathrm{H_2O}} \tag{8}$$

Single species concentrations in gas and liquid phase are considered in equilibrium, assumption (6), described by Henry's law for methanol and carbon dioxide. Moreover, gas phase is considered completely saturated by water:

$$C^{\mathrm{L}}_{\mathrm{Met}} = K_{\mathrm{H,Met}}C^{\mathrm{G}}_{\mathrm{Met}}RT \tag{9}$$

$$C^{\mathrm{L}}_{\mathrm{CO_2}} = K_{\mathrm{H,CO_2}}C^{\mathrm{G}}_{\mathrm{CO_2}}RT \tag{10}$$

$$C^{\mathrm{a,G}}_{\mathrm{H_2O}} = \frac{p^{\mathrm{H_2O}}_{\mathrm{sat}}}{RT} \tag{11}$$

Ideal gas mixture is assumed for gas phase, (6), thus, defining P^{a} as constant anode pressure, (7), Dalton equation relates gas phase concentrations:

$$C^{\mathrm{G}}_{\mathrm{Met}} + C^{\mathrm{a,G}}_{\mathrm{H_2O}} + C^{\mathrm{a,G}}_{\mathrm{CO_2}} = \frac{P^{\mathrm{a}}}{RT} \tag{12}$$

Ideal liquid mixture implies that total mass fraction in liquid phase is equal to 1:

$$C^{\mathrm{L}}_{\mathrm{Met}}\frac{M_{\mathrm{Met}}}{\rho^{\mathrm{L}}} + C^{\mathrm{a,L}}_{\mathrm{H_2O}}\frac{M_{\mathrm{H_2O}}}{\rho^{\mathrm{L}}} + C^{\mathrm{a,L}}_{\mathrm{CO_2}}\frac{M_{\mathrm{CO_2}}}{\rho^{\mathrm{L}}} = 1 \tag{13}$$

ρ^{L} is total density of liquid phase. It can be reasonably approximated equal to pure water density, $\rho^{0}_{\mathrm{H_2O}}$, considering that pure compounds densities are not very different from water value and compounds concentrations are limited to low values.

4.1.3. Anode diffusion layer

The sum of methanol fluxes in x direction, (3), is equal to the diffusive flow through the diffusion layer. The latter can be expressed as the sum of diffusive fluxes in both gas and liquid phases, assuming that void fraction is constant in y, within

diffusion and catalyst layers, (6):

$$\frac{i}{6F} + N_{\text{cross}}^{\text{Met}} = \frac{D_{\text{b}}^{\text{a,L}}}{l_{\text{b}}^{\text{a}}}(C_{\text{Met}}^{\text{L}} - C_{\text{t}}^{\text{L}})(1-\epsilon) + \frac{D_{\text{b}}^{\text{a,G}}}{l_{\text{b}}^{\text{a}}}(C_{\text{Met}}^{\text{G}} - C_{\text{t}}^{\text{G}})\epsilon \quad (14)$$

where $D_{\text{b}}^{\text{a,L}}$ and $D_{\text{b}}^{\text{a,G}}$ are effective methanol diffusivity in liquid and gas phases within the diffusion layer, C_{t}^{L} and C_{t}^{G} are methanol concentrations in the catalyst layer.

4.1.4. Anode catalyst layer

Time-averaged local concentration of methanol and gas-liquid equilibrium in the catalyst layer are defined similarly as in (6) and (9):

$$\bar{C}_{\text{t}} = \epsilon C_{\text{t}}^{\text{G}} + (1-\epsilon)C_{\text{t}}^{\text{L}} \quad (15)$$

$$C_{\text{t}}^{\text{L}} = K_{\text{H,Met}} C_{\text{t}}^{\text{G}} RT \quad (16)$$

Anode polarization is calculated assuming Tafel kinetic, (10), of order γ^{a}, depending on time-averaged local concentration of methanol in the catalyst layer:

$$\eta^{\text{a}} = \frac{RT}{\alpha^{\text{a}} F} \ln\left(\frac{i}{k^{\text{a}}}\right) \quad (17)$$

$$k^{\text{a}} = i_{*}^{\text{a}} \left(\frac{\bar{C}_{\text{t}}}{c_{\text{ref}}^{\text{a}}}\right)^{\gamma^{\text{a}}} \quad (18)$$

4.1.5. Membrane

Methanol and water crossover are due to liquid phase diffusion and electro-osmosis, assumption (9). Water and methanol concentrations at cathode side are negligible, in comparison to anode concentrations.

Electro-osmotic flux is proportional to current density, water drag coefficient of proton, n_{d}, and molar fraction of the involved species. Considering the abundant presence of water in the anode channel and the limited methanol concentration, the gradient of water concentration through the diffusion layer can be neglected. Thus, for simplicity, water concentration in the catalyst layer is assumed equal to anode channel one. Moreover, for the purpose of electro-osmotic flux calculation, water molar fraction in the catalyst layer is assumed equal to 1.

$$N_{\text{cross}}^{\text{Met}} = \frac{D_{\text{m}}^{\text{Met}}}{l_{\text{m}}} C_{\text{t}}^{\text{L}} + n_{\text{d}} \frac{i}{F} \frac{C_{\text{t}}^{\text{L}}}{C_{\text{H}_2\text{O}}^{\text{a,L}}} \quad (19)$$

$$N_{\text{cross}}^{\text{H}_2\text{O}} = \frac{D_{\text{m}}^{\text{H}_2\text{O}}}{l_{\text{m}}} C_{\text{H}_2\text{O}}^{\text{a,L}} + n_{\text{d}} \frac{i}{F} \quad (20)$$

Proton flow through the polymeric membrane produces a polarization, that obeys to the Ohm's Law; thus, considering the membrane perfectly hydrated and its conductivity, σ_{m}, constant in membrane domain:

$$\eta_{\text{ohm}} = i\left(\frac{l_{\text{m}}}{\sigma_{\text{m}}}\right) \quad (21)$$

Table 2
Geometrical parameters

h^{a} (cm)	0.08
h^{c} (cm)	0.08
L (cm)	76.6
l_{b}^{a} (cm)	0.01
l_{b}^{c} (cm)	0.01
l_{t}^{a} (cm)	0.001
l_{t}^{c} (cm)	0.001
l_{m} (cm)	0.018

Table 3
Experimental conditions

P^{a} (Pa)	101325
P^{c} (Pa)	101325
T (K)	333, 353
$\dot{m}^{\text{a}}$ (g min^{-1})	0.47, 1.08
$\dot{m}^{c}$ (dm^3 min^{-1})	0.2
C_{met}^{0} (wt.%)	3.25, 6.5
V_{cell} (V)	0.25–0.75

4.1.6. Cell potential difference

Potential difference across the cell is constant along z direction, as effect of electrodes equipotentiality, and is equal to the sum of anode, ohmic polarization and contact resistance voltage drop[1]:

$$V_{\text{cell}} = \eta^{\text{a}} + \eta_{\text{ohm}} + R_{\text{c}} i \quad (22)$$

4.1.7. Numerical solution

The system, composed by the equations from (3) to (22), presents three differential equations, 20 algebraic equations, 20 variables. This DAE system can be solved numerically, applying the appropriate initial conditions, regarding inlet flows, fuel cell temperature and potential difference. Total and mean electrical current can be calculated by integration over MEA area. These quantities permit to build polarization curves, commonly used to characterise direct methanol fuel cells. For this work Matlab®environment was used to solve the DAE system.

4.2. Validation

The quantities present in the model have physico-chemical meaning, there are no pure adaptive parameters. These quantities are divided in: geometrical parameters, defined by the experimental hardware, shown in Table 2; operating conditions, defined by experimental analysis, presented in Table 3; assumed parameters, provided by literature, Table 4; fitting parameters, Table 5.

The calibration procedure consists in minimisation of the residuals between model estimation and experimental results in the complete investigated range of operating conditions. The utilised experimental data are composed of 88 current density

[1] Contact resistance and cable voltage drop are measured and reported in Table 4.

Table 4
Assumed parameters

α^a	K_1	Calibration
c^a_{ref} (mol cm^{-3})	1×10^{-3}	[14,25]
$D^{a,L}_b$ (cm^2 s^{-1})	$0.7 \times 10^{-1.4163} - (999.778/T) \times 10^4$	[14]
$D^{a,G}_b$ (cm^2 s^{-1})	K_5	Calibration
D_m (cm^2 s^{-1})	$1.28 \times 10^{-6}\, e^{((2416/303)-(2416/T))}$	[26]
E_0 (V)	1.2	
F (C mol^{-1})	96495	
γ^a	K_4	Calibration
i^a_* (A cm^{-2})	$K_2\, e^{(K_3/R)((1/353)-(1/T))}$	Calibration
$K_{H,Met}$ (mol J^{-1})	$2.2\, e^{5200((1/T)-(1/298))}$	[27]
K_{H,CO_2} (mol J^{-1})	$3.5\, e^{2400((1/T)-(1/298))}$	[27]
n_d	$2.9\, e^{1029((1/333)-(1/T))}$	[23]
p_{sat} (MPa)	$-7.9((373/T)-1) - 1.38 \times 10^{-7}(10^{11.34(1-(T/373))} - 1) + 8.13 \times 10^{-3}(10^{-3.49((373/T)-1)} - 1) + 5.03 \log(373/T) + \log 1013$	[27]
R (J mol^{-1} K^{-1})	8.314	
R_c (Ω cm^2)	7.5×10^{-2}	Measure
ρ^L (g cm^{-3})	$= \rho^0_{H_2O}$	
$\rho^0_{H_2O}$ (g cm^{-3})	$(-0.0028(T-273)^2 - 0.1757(T-273) + 1003.8) \times 10^{-3}$	[27]
σ_m (Ω^{-1} cm^{-1})	$0.073\, e^{[1268((1/298)-(1/T))]}$	[23]

measures, coming from eight polarization curves, previously presented, at different temperature, inlet methanol concentration and inlet anode flow rate. The model is not intended to describe unsteady state behaviour, including hysteresis, thus its estimations are compared to mean data, characterised by final current density uncertainty, expanded by the hysteresis factor. Considering that the potential difference range interesting for applications is from 0.25 to 0.5 V, the calibration procedure was developed to produce a more accurate fitting in this range, where two-phase flow and methanol gas transport effects are still present. Moreover, at higher voltages complex two-phase fluid dynamics effects, not described by the model, may occur.

The fitting parameters, reported in Table 5, characterise anode kinetics and effective methanol diffusivity in gas phase through diffusion layer. The fitting parameters, K_1, K_2 and K_3, characterise anode kinetics, composed of quantities affected by high uncertainty, demonstrated by a high variability in literature [12,14,23,24]. The values resulting from calibration are reasonable and very similar to literature, in particular K_3 with [19,20]. The order of the overall anode reaction, K_4, is another uncertain parameter, in literature varies from 0 [14] to 0.5 [12] to 1 [11]. The value obtained by calibration, 0.02, is consistent with the experimental observation of a very weak current dependence on methanol concentration in the activation region, Fig. 6.

Considering the contribution of CO_2 counter diffusion, variation in void fraction and in methanol state equilibrium, the effective methanol diffusivity in gas phase through diffusion layer, K_5, is a considerably uncertain parameter. The fitting values result 40 times lower than that assumed in [14]. This difference is acceptable, considering the contribution and influence of the mentioned phenomena, moreover, the value is consistent with that obtained with the presented model and different experimental analysis, in [15]. In spite of a lower value of effective methanol diffusivity than expected, the model confirms that methanol diffusion in gas phase has a considerable role in transport through the diffusion layer.

Table 5
Fitting parameters

K_1	0.575
K_2 (A cm^{-2})	2.38×10^{-4}
K_3 (J mol^{-1})	73167
K_4	0.02
K_5 (cm^2 s^{-1})	3×10^{-3}

The residuals produced in the investigated interval, 0.25–0.5 V, between model estimation and experimental results have reasonably normal distribution and an absolute value inferior than 0.03A cm^{-2}, an example is reported in Figs. 10 and 11.

An accurate residual analysis has been effectuated, evaluating them in comparison with experimental uncertainty. In Fig. 12, the residuals are reported in function of current density, with relative experimental uncertainty. Model accuracy is evaluated quantitatively by F-test, as reported in [28]. It verifies if the model is sufficiently accurate, in comparison to experimental

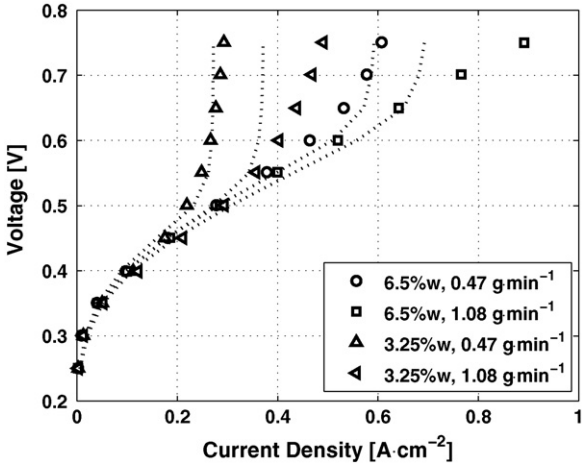

Fig. 10. Polarization curve experimental (points) and modelling (lines). Fuel cell temperature: 333 K; varying methanol concentration and anode flow rate.

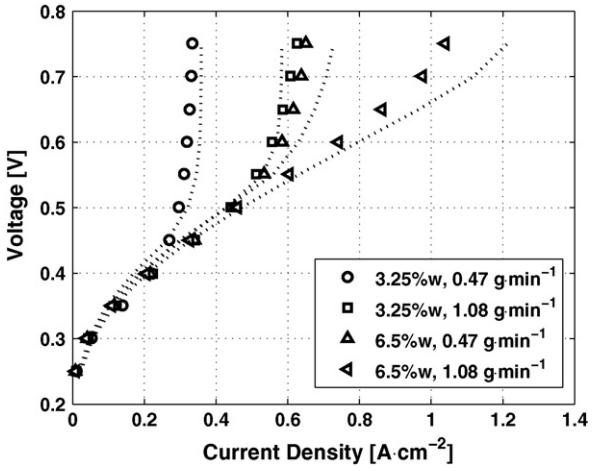

Fig. 11. Polarization curve experimental (points) and modelling (lines). Fuel cell temperature: 353 K; varying methanol concentration and anode flow rate.

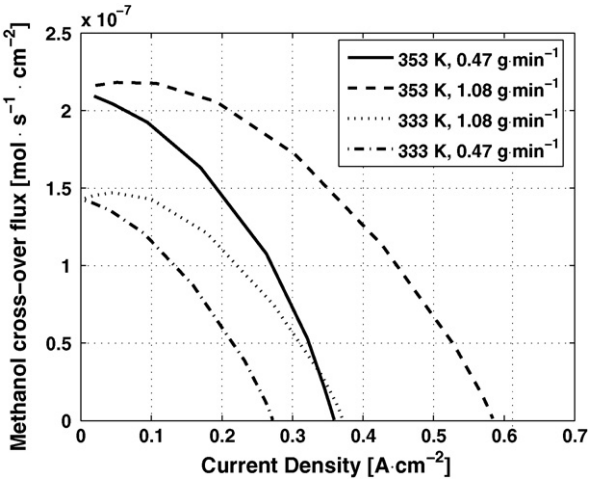

Fig. 13. Methanol crossover in function of current density. Methanol concentration: 3.25 wt.%; varying anode flow rate and fuel cell temperature.

uncertainty, to permit to consider the latter as confident interval of model estimation.

Experimental measures from 0.25 to 0.5 V satisfy *F*-test (95%), thus in this range the model results accurate in reproducing fuel cell behaviour and validated for prediction, maintaining experimental uncertainty as prediction confidence interval. This implies that the phenomena neglected with the proposed assumptions have minor effects. Measures having lower uncertainty are needed for a further evaluation of model accuracy. Instead above 0.5 V the model results less accurate, implying that predictions in that range have an error higher than experimental uncertainty.

4.3. Estimated quantities discussion

The model estimations of methanol crossover fluxes are qualitatively and quantitatively similar to measures reported in literature, Fig. 13. The order of magnitude and the approximately linear dependence on current density are consistent with experimental observations [7,21,22].

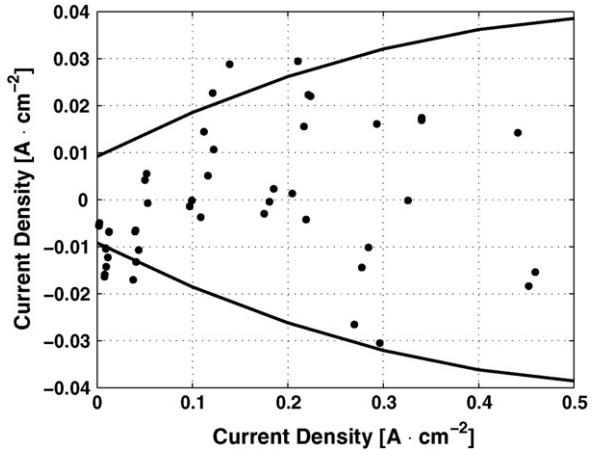

Fig. 12. Residuals in function of current density. Experimental uncertainty in solid line.

In Fig. 14, examples of local current density in function of channel length are reported. At low voltage current density is homogeneous along the channel, instead at high voltage it is more intense at fuel inlet, near 0.5 A cm^{-2}, and varies considerably along x. At 0.45 and 0.5 V, the transition from kinetics controlled region to transport controlled region is evident in the slope variation around, respectively, 500 and 150 mm. In these cases, current production near channel outlet results very limited as expected. In Fig. 15, where local methanol concentrations are reported in logarithmic scale, the same transition is appreciable at a methanol concentration about 1×10^{-6} mol cm^{-3}.

Void fraction increases rapidly along the channel; in the cases considered in Fig. 16 it reaches the value 0.5 at maximum within 30 mm and values very close to 1 at channel outlet.

In Figs. 17 and 18, total methanol flux through the diffusion layer, methanol flux in gas phase and the fraction associated to current production are presented. In the first example, methanol crossover, the difference between total flux and current flux, is very limited and present considerably in the first third of the channel. Different is the second case, where methanol crossover

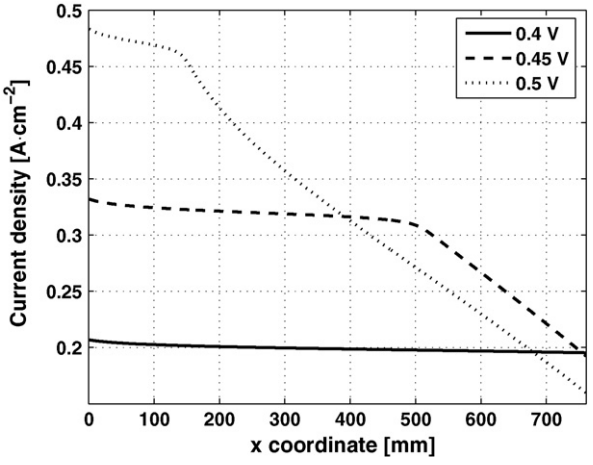

Fig. 14. Local current density in function of channel length. Methanol concentration: 3.25 wt.%; anode flow rate: 0.47 g min^{-1}; fuel cell temperature: 353 K.

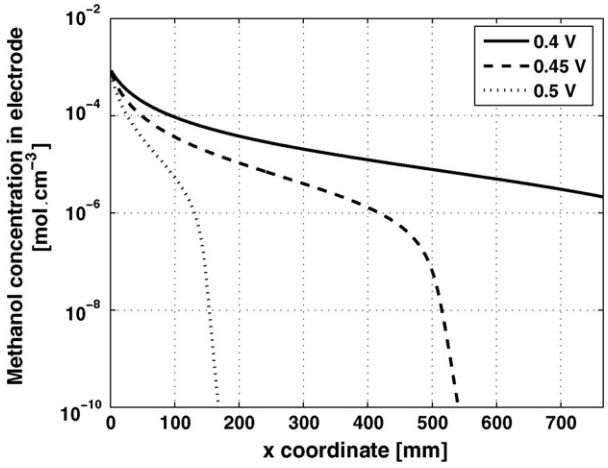

Fig. 15. Methanol concentration in the electrode in function of channel length. Methanol concentration: 3.25 wt.%; anode flow rate: 0.47 g min^{-1}; fuel cell temperature: 353 K.

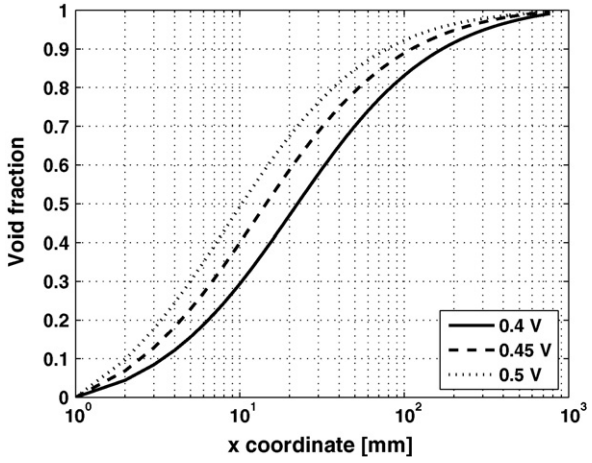

Fig. 16. Void fraction in function of channel length. Methanol concentration: 3.25 wt.%; anode flow rate: 0.47 g min^{-1}; fuel cell temperature: 353 K.

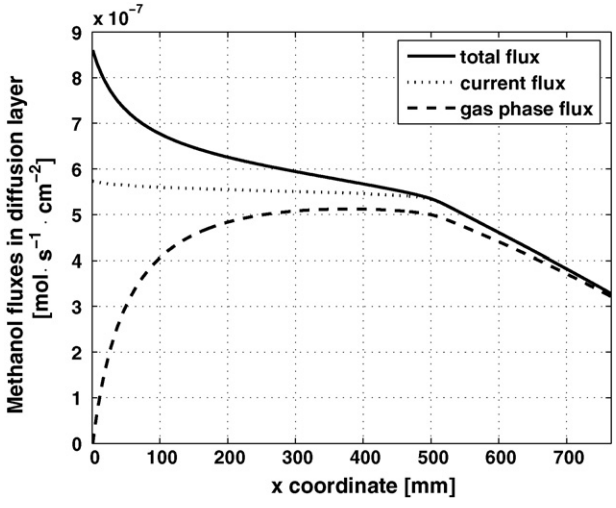

Fig. 17. Methanol fluxes in diffusion layer in function of channel length. Potential difference: 0.5 V; methanol concentration: 3.25 wt.%; anode flow rate: 0.47 g min^{-1}; fuel cell temperature: 353 K.

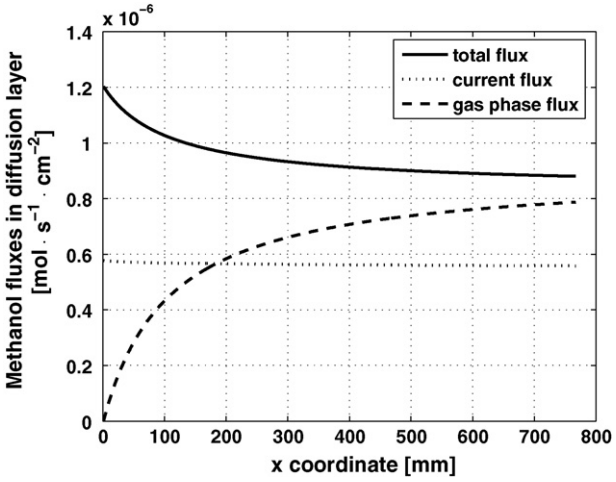

Fig. 18. Methanol fluxes in diffusion layer in function of channel length. Potential difference: 0.5 V; methanol concentration: 6.5 wt.%; anode flow rate: 1.08 g min^{-1}; fuel cell temperature: 353 K.

is always more than 30% of the total flow in the diffusion layer, reaching 50% at channel inlet. Regarding gas phase transport it is important to observe that it seems to produce the predominant contribution, excluding channel inlet. Moreover, its importance is evident also in the second case, despite the cell is fed with a very large methanol stoichiometry; in both cases more than 80% of the flux through the diffusion layer in the second half of the channel is due to gas phase transport.

These observations confirm the important contribution that methanol transport in gas phase has in feeding the electrode and emphasise the possibility to optimise related aspects, in particular diffusion layers, to reduce methanol crossover and to enhance fuel cell performance.

5. Conclusions

The analysis presented in this work produces the following conclusions:

- A systematic experimental analysis of operating conditions influence on anode polarization is presented, characterising measurements in term of uncertainty and reproducibility.
- Influence of operating condition history on performance is observed: a hysteresis effect on current measured values, decreasing and increasing voltage. Experimental results confirm that it arises from methanol accumulation; consequently this phenomenon has to be considered in evaluating DMFC performances uncertainty and reproducibility of measurements.
- Methanol electro-oxidation kinetics results weakly dependent on methanol concentration.
- The developed model has been calibrated in an extensive operating condition range, utilizing 48 current density measures, coming from eight polarization curves, and determining five fitting parameters.
- The proposed model reproduces accurately DMFC anode polarization in the investigated range. The obtained val-

ues of fitting parameters and local quantities estimation are consistent with literature and the residuals between model estimations and experimental results are inferior to measurement uncertainty.
- Both experimental results and model estimations confirm the important contribution of gas phase methanol transport in anode feeding. Moreover. they emphasise the possibility to optimise anode flow rate in order to improve DMFC performance and reduce methanol crossover.

References

[1] A.S. Aricò, S. Srinivasan, V. Antonucci, Fuel Cells 1 (2001) 133.
[2] A. Heinzel, V.M. Barragan, J. Power Sources 84 (1999) 70.
[3] T. Bewer, T. Beckmann, H. Dohle, J. Mergel, D. Stolten, J. Power Sources 125 (2004) 1.
[4] H. Yang, T.S. Zhao, Q. Ye, J. Power Sources 139 (2005) 79.
[5] G.Q. Lu, C.Y. Wang, J. Power Sources 134 (2004) 33.
[6] K.Y. Jina, H.W. Hia, W.S. Ihla, L.H. Keeb, J. Power Sources 159 (2006) 491.
[7] H. Dohle, J. Divisek, J. Mergel, H.F. Oetjen, C. Zingler, D. Stolten, J. Power Sources 105 (2002) 274.
[8] B. Gurau, E.S. Smotkin, J. Power Sources 112 (2002) 339.
[9] H. Dohle, K. Wippermann, J. Power Sources 135 (2004) 152.
[10] A.A. Kulikovsky, J. Appl. Electrochem. 30 (2000) 1005.
[11] J. Ge, H. Liu, J. Power Sources 160 (2006) 413.
[12] A.A. Kulikovsky, Electrochem. Commun. 7 (2005) 237.
[13] J. Ge, H. Liu, J. Power Sources 163 (2007) 907.
[14] Z.H. Wang, C.Y. Wang, J. Electrochem. Soc. 150 (2003) 508.
[15] A. Casalegno, PhD Thesis, Politecnico di Milano, 2007.
[16] Env 13005:1999, BIPM, IEC, IFCC, ISO, IUPAC, IUPAP, OIML. International Organization for Standardization, ISBN 92-67-10188-9, First Edition, 1993.
[17] B.N. Taylor, C.E. Kuyatt, NIST Technical Note 1297, National Institute of Standards and Technology, 1994.
[18] A. Casalegno, R. Marchesi, F. Rinaldi, ASME J. Fuel Cell Sci. Techonol. 4 (Nov. 2007).
[19] T. Schultza, K. Sundmacher, J. Power Sources 145 (2005) 435.
[20] S.Lj. Gojkovic, T.R. Vidakovic, D.R. Durovic, Electrochim. Acta 48 (2003) 3607.
[21] A. Casalegno, P. Grassini, R. Marchesi, Appl. Thermal Eng. 27 (2007) 748.
[22] V. Gogel, T. Frey, Z. Yongsheng, K.A. Friedrich, L. Jrissen, J. Garche, J. Power Sources 127 (2004) 172.
[23] K. Scott, W. Taama, J. Cruickshank, J. Power Sources 65 (1997) 159.
[24] H. Guo, C.F. Ma, Electrochem. Commun. 6 (2004) 306.
[25] R. Chen, T.S. Zhao, J. Power Sources 152 (2005) 122.
[26] H. Dohle, J. Divisek, R. Jung, J. Power Sources 86 (2000) 469.
[27] Nist standard reference database 106. IUPAC-NIST Solubility Database, 2003.
[28] D.M. Himmelblau, Process Analysis by Statistical Methods, Wiley & Sons, 1970.